Int. J. Heat Mass Transfer. Vol. 24, pp. 407–419
Pergamon Press Ltd. 1981. Printed in Great Britain

0017-9310/81/0301-0407 $02.00/0

HEAT TRANSFER FROM A ROW OF IMPINGING JETS TO CONCAVE CYLINDRICAL SURFACES

PETER HRYCAK
Mechanical Engineering Department, New Jersey Institute of Technology, Newark, NJ, U.S.A.

(*Received* 15 *February* 1980 *and in revised form* 2 *June* 1980)

Abstract – Starting from the first principles, and with one experimentally obtained parameter, an expression for stagnation heat transfer is derived, applicable to round, impinging jets. The results obtained with a row of air jets impinging on an electrically-heated surface in a small-scale setup characteristic of a typical turbine blade, have been found compatible with the average heat transfer from a geometrically similar, steam-heated surface scaled up ten times, and comparable with the results of other investigators. These findings were linked to the flow fields likely to exist in the gas turbine blades, internally cooled by a row of round jets or a single jet of equivalent width. The magnitude of heat-transfer coefficients obtained here with impinging jets approaches that normally associated with forced convection of water and evaporative cooling.

NOMENCLATURE

a, free constant in Froessling's solution [s^{-1}];
a^*, slope of dimensionless velocity profile plotted vs dimensionless distance from stagnation point, $aD/u_{oc} = \Delta(v/u_{oc})/\Delta(r/D)$ at $r = 0$;
b, outer boundary-layer thickness of wall jet, or equivalent slot width $\pi D^2/4C_n$[m];
C_f, friction coefficient;
C_n, nozzle center-to-center spacing [m];
c_p, specific heat at constant pressure [J/kg K];
D, nozzle diameter [m];
D_c, calorimeter diameter [m];
D_p, plate diameter [m];
Fr, Froessling number, $Fr \equiv Nu/Re_D^{0.5}$;
h, heat-transfer coefficient [$W\,m^{-2}\,K^{-1}$];
k, thermal conductivity [$W\,m^{-1}\,K^{-1}$];
L, significant length [m];
Nu, Nusselt number, hL/k;
Pr, Prandtl number, $c_p\mu/k$; $Pr = 0.72$ used in getting numerical constants, equation (5) ff.
St, Stanton number, $Nu/RePr$;
r, s, distance away from center of symmetry [m];
Tu, turbulence intensity; $[(u'^2 + v'^2 + w'^2)/3]^{1/2}/u_{oc}$;
Re_L, Reynolds number, $u_{oc}L/\nu$;
u, axial jet velocity [m/s];
v, radial jet velocity [m/s];
Z, distance away from target plate [m].

Greek symbols

δ, boundary-layer thickness [m];
μ, dynamic viscosity [kg/ms];
ν, kinematic viscosity [m^2/s];
ξ, $(Z - \delta)/b$, similarity variable.

Subscripts and other symbols

o, referring to origin or stagnation point;
c, referring to center of symmetry;
m, w, fluid medium, wal conditions, respectively (for temperature dependent properties);
$\bar{}$, average value;
m, condition where velocity is maximum;
n, normal distance away from target plate in Z_n/D expression;
$'$, indicates differentiation, or fluctuating velocity component in turbulent flow;
ssc, referring to small-scale configuration.

Additional symbols explained in text.

INTRODUCTION

IN MANY applications where surface cooling of vital machinery components is required today, it becomes necessary to provide a particularly vigorous spotcooling effect which cannot be produced by conventional convective cooling methods, or without a change of phase of the cooling fluid. In such cases, cooling by impinging jets seems to provide often the best answer. In particular, the impinging jets seem to be very suitable for gas turbine applications. Likewise, for steam turbines capable to operate at temperatures exceeding the present metallurgical limit, the possibility of internal cooling of the blades by means of jets appears very attractive. The obvious alternatives, like, for example, blowing and the use of porous surfaces, have inherent disadvantages from the point of view of durability and routine maintenance. For cooling of areas of larger extent, application of rows of impinging jets are quite suitable [1].

Unfortunately, there is still relatively little experimental information available in the area of cooling by

impinging jets. It is intended here to discuss the additional results produced at NJIT as a direct continuation of an earlier discussion [2], related to the analysis of flow patterns of jets, both free and impinging, in order to bring about a better understanding of the mechanism behind cooling of cylindrical concave surfaces by jets, operating individually and in groups. Because of its relatively late appearance on the scene, heat transfer from impinging jets is not as well established in the literature as are its more conventional forms. Also, while the results of a substantial number of investigations of heat transfer from jets impinging on flat surfaces have been reported (cf. [1, 3–8]), there appeared only relatively few experimental results concerning heat transfer from the jets impinging on concave surfaces [9–16]. A notable exception here is the monograph by Shvets and Dyban [17] with a bibliography of 439 items, about one third of them in English.

As a typical example of a study of heat transfer to concave surfaces may serve measurements of average and local heat-transfer rates between rows of impinging circular jets and a concave cylindrical surface by Metzger *et al.* [9]. It was found that, for the center-to-center nozzle spacing C_n of 1.67 to 6.67 nozzle diameters, a maximum in the average heat-transfer coefficient was observed for the nozzle-to-target distance of about one nozzle diameter. Such a short nozzle-to-plate distance appears to be characteristic for maximum heat transfer from the multiple jets, as opposed to measurements made with a single impinging jet, where the maximum usually occurs at $Z_n/D \approx 7$ [1].

A substantial number of investigators have treated particular areas of interest, like for example, the wall jet friction [18]. Of significant interest was also the problem of a developing jet associated with the effects of disappearance of potential core some four to seven diameters downstream from the nozzle [19–22] and the wall-jet patterns encountered when impinging surfaces had a curvature [23–25]. Of great help in finding solutions to the governing differential equations was Schlichting's monograph on the boundary-layer theory [26]. In the present investigation, flat plate was used to determine the general fluid flow and heat-transfer patterns, the large-scale configuration served to determine local and average heat-transfer results, while the small-scale configuration provided a general check on the overall heat-transfer data obtained here and from the literature.

THE APPARATUS

The jet flow patterns (Fig. 1) have been investigated by means of an array of total and static pressure probes of conventional design (Fig. 2), and by using a number of pin-hole pressure taps arranged orderly in rows at right angles to each other on the impinging surfaces [19]. The probes were supported on stages with a positioning accuracy of 0.15 mm; they could also be rotated around three mutually perpendicular axes. Air, filtered and de-humidified, was supplied by compressors at around 3 atm abs. Air volume was measured by high precision rotameters.

The experimental setup for heat transfer measurements from impinging jets, both individual and in rows, differed in plenum chamber arrangements, and the number of rotameters used. A typical general experimental setup appears in Fig. 3, and a calorimeter for measuring the resulting heat flux is shown in Fig. 4. Generally, electrically generated steam, condensing at atmospheric pressure inside of an appropriately insulated container, was used to heat the target plate. For the small-scale configuration, guarded-type electrical heater was provided, whose electrical input was used to measure the average heat transfer (Fig. 5).

Large-scale configuration setup details may be found in Fig. 6 and in [2]. Local heat transfer was measured by means of cylindrical calorimeters, insulated by an annular air gap on the side, of various sizes and diameters. The calorimeters used for heat-transfer measurements on the semicylindrical plate were made of 304 stainless steel, and had dia. of 5.08 mm, a height of 12.7 mm, and two holes for fine wire thermocouples drilled on one side. They were secured to the support plate by a nut and screw arrangement brazed on to the bottom. High conductivity silicon grease was used to minimize contact resistance to the plate (Fig. 4), while an annular air gap minimized heat leaks through the calorimeter walls. The calorimeter shown in Fig. 4 was very similar to the ones used in the flat plate experiments. These calorimeters were developed after several years of experimentation with the target plates of a relatively simple geometry, to generate reliable thermocouple readings which were evaluated by a high precision potentiometer. Because of the simplicity of the basic calorimeter geometry, the fact that they were made from metal whose conductivity was determined by the National Bureau of Standards,† and a quite small thermocouple wire conductance error, no separate calibration of the calorimeters was carried out. Instead, the calorimeter-related results were checked from independent fluid flow measurements and by analytical means wherever possible; wall-jet heat transfer was based on a semi-empirical theory using Colburn's analogy. These are the most characteristic features of the present investigation.

The calorimeter heat-transfer flux could be calculated in the steady state from the temperature gradient established by the two thermocouples located in the holes shown in Fig. 4 and the thermal conductivity of the metal used (here 304 stainless steel, chosen on purpose as a poor conductor to generate substantial, easily measurable, temperature differences). Then, t_w, the surface temperature, was calculated from the known calorimeter temperature gradient by extrapolation, and the heat-transfer coefficient from setting

† By special arrangement.

$h(t_m - t_w)$ equal to the calorimeter heat flux. Relatively large number of the calorimeters used for the cylindrical surface (21), and the fact that only the central one-fifth portion of the heated target surface exposed to the cooling action from the nozzles was used for heat-transfer measurements, should have enhanced the reliability of the experiment by elimination of the end effects in both the temperature distribution, and in the flow fields of the resulting wall jets.

The plenum chambers used for the multiple jet experiments were of unique design [2], insulated with flannel and covered with reflective insulation. They were similar to the plenum chamber in Fig. 5, except that air was supplied to the top of the chamber by two ducts branching off from a common 'settling chamber'. Tightly-packed glass wool, supported by expanded metal screen, insured equal air distribution inside of the plenum chambers, and a uniform discharge through the openings simulating typical jet nozzles. These were square-edged holes with dia. of 9.52, 6.35 and 3.18 mm with openings located from one to seven diameters from each other, along the entire bottom of plenum chambers. Thus the plenum chamber holes formed nozzles, closely resembling the nozzles likely to occur in actual applications. Three rows of calorimeters, with seven in each row, located symmetrically across the semicylindrical impingement plate, were provided to measure local heat transfer. The use of a grinder bed as the test stand support (Fig. 3) allowed to align the plenum chambers precisely with the target plate and to be brought into fixed positions away from it within 0.05 mm. The measurements were carried out for a number of dimensionless distances, Z_n/D, away from the plate. Experience with the single jets showed

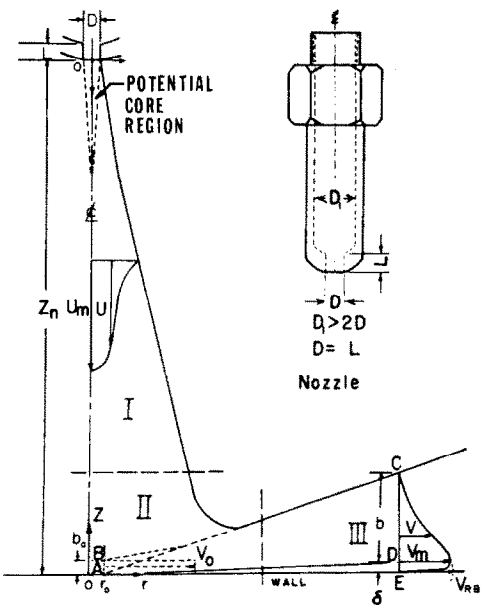

FIG. 1. Fluid flow regions in an impinging jet. A nozzle detail (used in single jet, flat plate experiments).

that the Nusselt number due to an impinging jet is a function of Z_n/D, of the location of the calorimeter with respect to the centerline of the jet nozzle, and of the Reynolds number. For the Reynolds numbers based on the size of the openings in the plenum chamber Re_D, the experimental setup described above could produce Reynolds numbers up to 30 000, for the plenum chamber with the largest available free area for air flow. This limitation was due to the combined capacity of the then available compressors (a total of 40 h.p.).

It was also obvious that the interference effects from the adjacent jets had to be considered. The effect of the distance from the jet nozzle to the impingement plate, and of the distance away from the stagnation point along the plate itself on the resulting wall jet, had to be treated separately. The particular flow regions are shown in Fig. 1. The apparatus used appeared to be flexible enough to provide information on each of the three zones in Fig. 1. Experiments with a single jet, impinging on a flat plate, were used as a step towards a better understanding of multiple jet phenomena and of the effects of curved surfaces on impinging jet heat transfer, being easier to treat analytically.

CALCULATION OF HEAT TRANSFER FROM EXPERIMENTAL RESULTS

Heat-transfer patterns at the stagnation point can be explained with the help of axisymmetric stagnation flow theory of ideal fluid and the exact solutions of the Navier–Stokes equations due to Homann and Froessling [26]. Comparisons with the results of approximate theory as outlined by Pohlhausen [26] and Eckert and Drake [27] lead to a better understanding of the basic physical processes involved. Here, very helpful are the related fluid flow measurements. Thus, experiments with single jets impinging on a flat plate show a maximum Nusselt number for $Z_n/D \approx 7$ [1], while our own measurements showed that this coincided roughly with the end of the nominal potential core region [21] (Fig. 1) and the great intensity of turbulence there [3, 20]. The results for impingement on concave surfaces showed, however, deviations from the previous flow patterns for the same Reynolds numbers, due to what appeared to be a still greater turbulence intensity [24] which manifested itself in several ways. Independent experiments with internal turbulence promoters (Dyban and Mazur [22]) have shown a very substantial shortening or even virtual disappearance of the potential core for turbulence intensities up to $Tu = 25\%$. This explains the fact that for optimum heat transfer for rows of jets on concave surfaces, Z_n/D magnitude is substantially less than seven, normally associated with the nominal tip of the potential core. The true potential core length has been determined in [21] as being about 4 + diameters long, for normal impingement on flat surfaces without the use of turbulizers [8, 21].

Figure 2 shows the experimental verification of the fact that, for $r < 1.5\,D$, the hydrodynamic boundary-layer thickness is independent of r at the center of

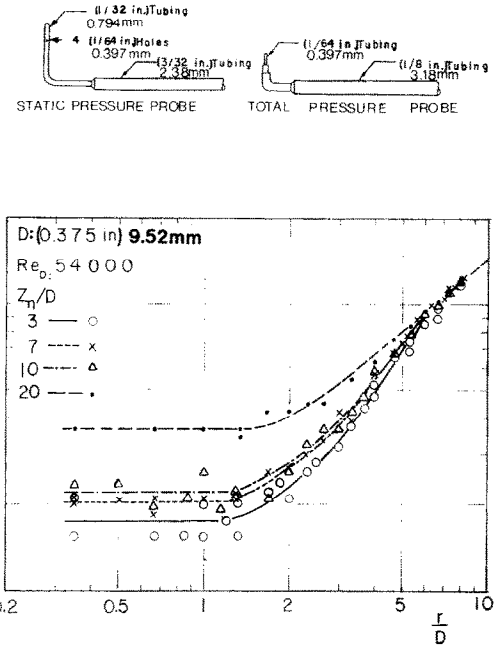

FIG. 2. Boundary-layer development at stagnation point and transition to wall-jet flow on a flat plate. The probes used.

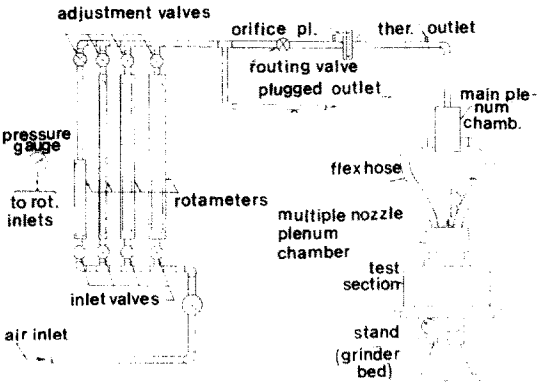

FIG. 3. General experimental setup for large-scale configuration, concave semi-cylindrical plate.

symmetry of the tangential plane. Moreover, for the velocity distribution inside the boundary layer of the form $v/v_m = \phi'$, one gets for the boundary-layer thickness an expression of the form (cf. Froessling [26])

$$\delta/D = 1.98/(a^* Re_D)^{1/2} \tag{1}$$

while $\phi''(0) = 1.312$ describes velocity gradient at the impingement surface, and where $a^* = \Delta(v/u_{oc})/\Delta(r/D)$ can be obtained experimentally by plotting velocity outside of the boundary layer vs. distance. Measurements showed, however, that the actual thickness of the viscous layer, δ, may be 50–100% larger [19, 20], due to a highly turbulent flow in the potential flow region of the jet near the critical point where the flow lines are turning (Fig. 2). An independent observation of this phenomenon was made also by Dyban and Mazur [22]. Thus, δ represents only the viscous sublayer of otherwise turbulent flow. It is of some interest to compare the exact solutions of the governing differential equation here as due to Homann and Froessling with alternate methods. Thus, on using the method outlined by Pohlhausen ([26], p. 240), based on a 4th power polynomial, the constant in equation (1) is found to be 2.17, whereas $\phi''(0) = 1.289$ applies then at the wall. Using a 3rd degree polynomial and the procedure suggested by Eckert [27], the constant in equation (1) becomes 1.87 and $\phi''(0) = 1.269$, which gives correctly the form and the order of magnitude of the boundary-layer thickness and of the shear-stress near the wall, at the stagnation point for an axisymmetric flow due to an impinging jet.

To calculate heat transfer at the stagnation point, it appears that Froessling's solution can be used again, in the form as shown in [26] p. 100, where $\phi' = v/v_m \sim (T - T_m)/(T_w - T_m)$, with $q = h(T_m - T_w)$, and $v = ar$. Here, $q = -k(\partial T/\partial z)_{z=0}$ also applies; moreover, one can choose for the viscous layer here a proportionality constant $Pr^{0.39}$ between the velocity and the temperature profiles, adapted from Sibulkin's solution for heat transfer near the stagnation point on a sphere [28]. In this fashion, an expression for stagnation point heat transfer is obtained, with a free constant, a:

$$q = -0.697k[\phi''(0)]^{1/3} Pr^{0.39} (a/v)^{1/2} (T_w - T_m). \tag{2}$$

Since $a^* = aD/u_{oc}$, and $\phi''(0) = 1.312$, equation (2) yields

$$Nu_0 = 0.763 Pr^{0.39} (a^* u_{oc} D/v)^{1/2}. \tag{3}$$

From cross-plotting of the flat plate results from [19] (Fig. 7), one gets here $a^* = 32.6/(Z_n/D)^{1.75}$, in the interval $Z_n/D > 7$.

In Appendix I another approach to determine the magnitude of a^* is suggested for small Z_n/D values, where it is shown that both the experimental values and the potential flow solutions for a^* tend towards unity as $Z_n/D \to 1.0$. Since the experimentally obtained a^* decreases with Z_n/D, while corresponding heat-transfer measurements show for $2 \leq Z_n/D \leq 7$ an increase in Nu_0[1, 3], the following procedure appears appropriate. In equation (3), a^* is replaced by $(Z_n/D)^{2n}$, n being an experimentally obtained exponent. Then, the actual behavior of a typical nozzle can be closely duplicated (for example, cf. Fig. 3 of [1]). In addition, the effects of turbulence downstream of the nozzle will be approximated. Our own flat plate experiments indicate $n = 0.16$ (Fig. 7) for $2 \leq Z_n/D \leq 7$, which applied to the above Z_n/D ratio, on substitution in equation (3), yields for heat transfer at the stagnation point the expression

$$Nu_0 = 0.763 Pr^{0.39} Re_D^{1/2} \times (Z_n/D)^{0.16}, \; 1.5 \leq Z_n/D \leq 7. \tag{4}$$

It is generally understood that the term $(Z_n/D)^{0.16}$ represents in a sectionally continuous form the effects of turbulence outside of the viscous layer δ on stagnation point heat transfer; it is the only empirical parameter on which equation (4) appears to depend explicitly, although there is also an implicit dependence on a^*. Since, conceivably, a^* may be intimately related to the individual nozzle characteristics, it may affect the exact numerical value of the constants used in equation (4) somewhat. Equation (4) represents the magnitude of the stagnation point heat-transfer intensity that is to be compared with the experimentally obtained expression for Nu_o (cf. equation (13) of [2], which is 81% higher; it can be seen from Fig. 2 of [22] that this corresponds to a turbulence intensity of the jet of 18%. Equation (5)

$$Nu_o = 1.42\, Pr^{0.39}\, Re_D^{1/2}\, (Z_n/D)^{0.16}\, (D/D_c)^{0.28} \quad (5)$$

is applicable for $D > D_c$ and $Z_n/D \leq 7$ (Fig. 7). Since turbulence level in impinging jets appears to be the greatest near $r = 0$ at the stagnation point outside of the viscous layer given here by equation (1), experiments have shown a local heat-transfer dependence on the ratio D/D_c, in spite of the fact that δ/D itself is not a function of r for small r-values; $\overline{Z_n/D} = 1.5$ that appears above in connection with the calculation of $\bar{a}^*$ is practically the lowest Z_n/D value where the presence of the impinging plate still does not affect the jet behavior at the nozzle [19, 20]. On the other hand, experiments show that average heat transfer here is mainly affected by the wall jet flow, cf. Zone III of Fig. 1. There, in the inner layer of wall jet zone applies the relation

$$v/v_m = (z/\delta)^{1/n} \quad (6)$$

with $7.5 < n < 15$ (cf. [19] and [20]); in the outer layer, $\delta < z < b$, experimental measurements have produced consistently an expression that appears to be independent of the effects of curvature (cf. Fig. 4), except in the region farther away from the impingement surface,

$$v/v_m = (1 - \xi^{1.5})^2 \quad (7)$$

and for the maximum velocity decay [20], one has

$$v_m/u_{oc} = 1.4\, (r/D)^{-1.12}. \quad (8)$$

Equations (6) and (7) have some theoretical background, but must be considered as convenient empirical approximations in the present case. In equation (6), please note the relatively high n-values for $Re_D < 10^5$, in comparison to the conventional flat plate flow. Equation (8) has been obtained theoretically [19, 20]. Consequently, it is to be expected in the wall-jet region that heat transfer shall be somewhat different from that associated with a flat plate flow at zero incidence, because of different velocity profiles.

It is interesting to note that the presence of curvature on the impinging plate does not greatly affect the observable characteristics of the wall jets. Thus, for the flat plate the relation $\delta = 0.1b$ applies, with $b = 0.22\,(r - r_o)$, and, for a sufficiently high value of Re_D, one has [19, 20]

$$\delta/D = 0.0175\, (r/D)^{0.95} \quad (9)$$

independent of the Reynolds number and (Z_n/D) (as seen in Fig. 2 for $r/D > 8$), while $\delta = b/18$ and $b' = 0.223$ are good for the concave hemisphere [24] and $\delta = 0.1b$, $b' = 0.23$ for a convex hemisphere [25], where the constant in the equation equivalent to equation (9) varies from 0.019 to 0.025, depending on the Reynolds number. The empirical formula for velocity distribution on convex hemisphere [25] is very similar to the plot given by equation (7) here (cf. Fig. 4). From comparison of velocity distribution in the wall jet on the flat plate [19, 20] with those on concave [24] and convex [25] surfaces, one sees a lot of similarity, particularly in the region associated with v_m. Therefore, one could expect that there would be also basic similarities in the associated heat transfer. As may be expected, velocity distribution farther away from the curved target surface depends on its radius of curvature, which fact may also have some influence on the general character of heat transfer in the resulting wall jets. The effect of curvature on the thickness of the inner layer, δ, is substantial, however. Outside of the stagnation region, one can use the Colburn analogy approach, with C_f due to Poreh *et al.* [18], to estimate wall-jet heat transfer

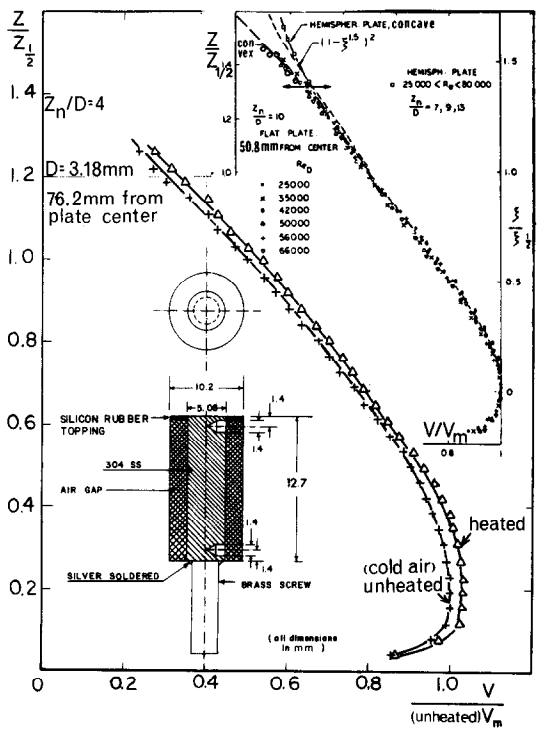

FIG. 4. Details of calorimeters used. Comparison of wall-jet velocity distribution for several geometries showing effects of curvature, with and without wall heating.

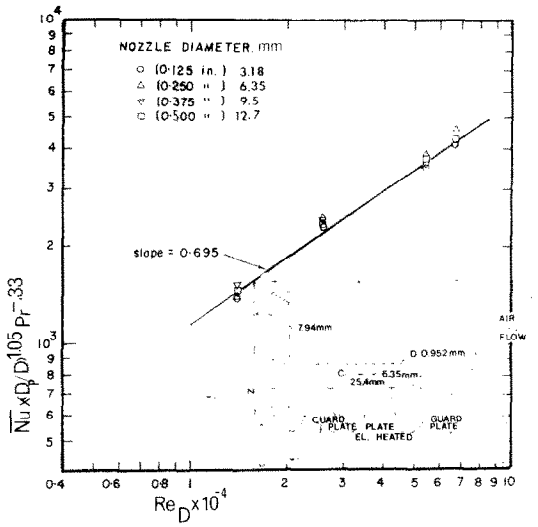

FIG. 5. Small-scale configuration plenum chamber and heating elements arrangement (bottom guard plate not shown). Average Nusselt number vs. Reynolds number, flat plate (D_p = 152.4 mm).

$$St\,Pr^{2/3} = C_f/2 = 0.06\,(v_m\delta/\nu)^{-0.3}\,(r/Z_n)^{-0.16} \quad (10)$$

and using equations (10), (8) and (9), after integration and a few simple transformations, one obtains an expression from which heat transfer in the wall jet region can be calculated, namely

$$Nu = 1.9\,Pr^{0.33}\,Re_D^{0.7}\,(D/D_p)^{1.23}. \quad (11)$$

The average Nusselt number, $\overline{Nu}$, is independent of

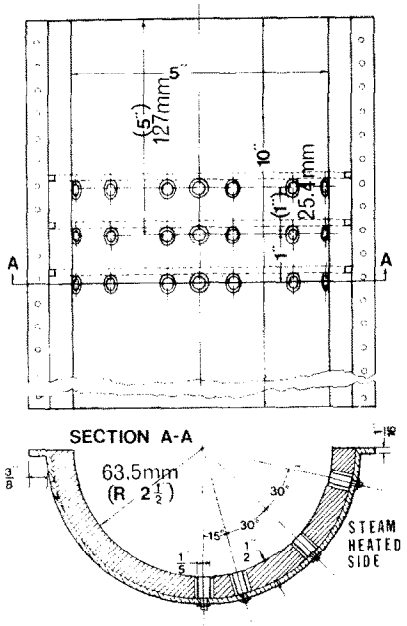

FIG. 6. Calorimeter arrangement on steam-heated, semi-cylindrical plate (large-scale configuration).

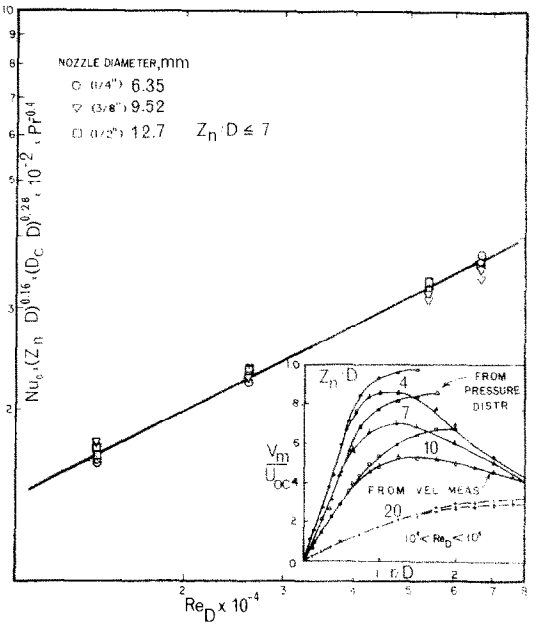

FIG. 7. Stagnation point Nusselt number vs. Reynolds number, flat plate. Maximum velocity distribution near stagnation point and beginning of wall jet formation.

Z_n/D for $Z_n/D \leq 7$, but depends inversely on the plate diameter. The experimental results come close to equation (11) except for a minor difference in D/D_p power (Fig. 5)

$$\overline{Nu} = 1.85\,Pr^{0.33}\,Re_D^{0.695}\,(D/D_p)^{1.05}. \quad (12)$$

Of particular interest here is a very close similarity in the power of the Reynolds number between the calculated and the experimental results on the flat plate, with a dia. of 152.4 mm. An alternate form of equation (11) is in Appendix II.

EFFECTS OF NON-ISOTHERMAL CONDITIONS

The effect of temperature gradients, naturally occurring when heat transfer takes place, based on fluid-flow calculations carried out with isothermal fluid, can in principle be assessed through dimensional analysis. In addition to the purely geometrically related parameters, the Nusselt number will depend on ρ, μ, k, and c_p temperature-related changes. Since the Prandtl number is virtually temperature independent, for the effect of the particular temperature-dependent parameters one can write, for example

$$\frac{\rho_m}{\rho_w} = \frac{T_w}{T_m};\ \frac{\mu_m}{\mu_w} = (T_m/T_w)^n = \frac{k_m}{k_w}.$$

Then the entire temperature dependence of Nu can be expressed in terms of a factor $\psi = T_m/T_w$ raised to a power n; $n = -0.25$ is recommended by some authoritities [29]. Fluid-flow measurements carried out on a heated plate with $T_m - T_w = 60$°C are

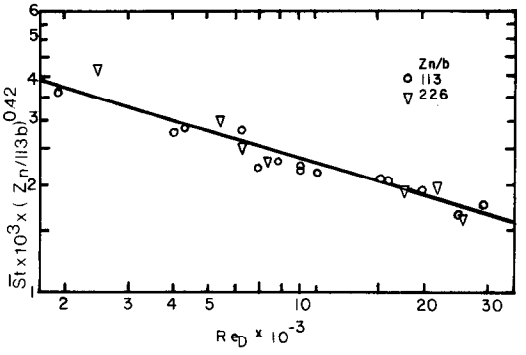

FIG. 8. Average heat transfer, small-scale configuration.

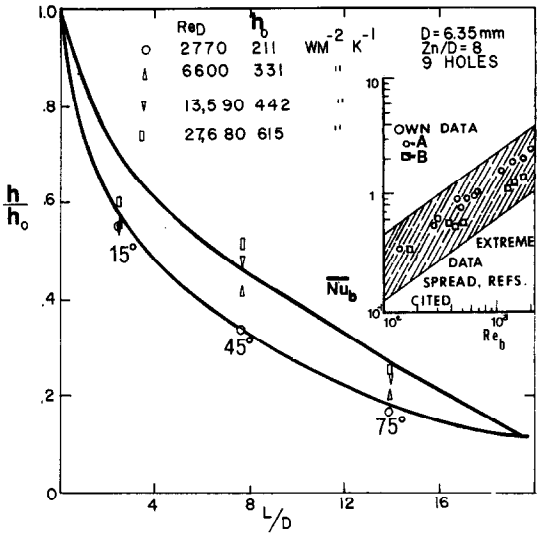

FIG. 9. Local distribution of heat-transfer coefficients. Small-scale configuration data comparison with references used; (A) $Z_n = 12.7$ mm; (B) $Z_n = 25.4$ mm; cylinder dia.: 12.7 mm.

compared with cold air results in Fig. 4; here, for $\psi = 1.2$, the experimental non-isothermal measurements differ only very little from the ones carried under isothermal conditions, virtually still within the limits of the experimental error (5%) considered acceptable. Temperature dependence of Nu can be more closely determined by introducing equation (12) into the given formulas directly, and then performing some mathematical manipulations. It may be shown that then the applicable power of T_m/T_w will depend on the actual power of Re_D particular to the given formula.

EXPERIMENTAL RESULTS, SMALL-SCALE CONFIGURATION

Small-scale configuration test setup was a scaled-down (by a factor of 10) version of the principal heat-transfer experimental apparatus. Only average heat transfer was measured, for two Z_n/b ratios, 113 and 226, and for just one orifice size, $D = 0.952$ mm. The Reynolds number range covered was $2500 < Re_D < 30000$, with nozzle spacing $C_n/D = 6.67$. The working temperature difference used amounted to 10–13°C. The experimental results are shown in Fig. 8, where the Stanton number St follows the relationship

$$St = 0.0372\, Re_D^{-0.3}\, (Z_n/113b)^{-0.42} \qquad (13)$$

which leads to an average Nusselt number

$$\overline{Nu}_{D,\,ssc} = 1.04\, Pr \times Re_D^{0.7}(Z_n/b)^{-0.42}(C_n/D)^{-0.16}(D/D_p)^{0.402} \qquad (14)$$

where, for the sake of a better direct comparison with the semicylindrical plate results, also the terms C_n/D and $D/D_p = 3/40$, have been included, that were not varied in the small-scale configuration experiments. The required powers for these two terms come from semicylindrical plate experiments. The particular dependence of the average heat transfer here on Z_n/b (equivalent to $Z_n/D = 13.3$ and 26.7) is affected by a large nozzle-to-plate distance. Comparison with the results of other investigators is best made via the effective slot width, $b = \pi D^2/4C_n$, which also lowers the order of magnitude of Re_b relative to Re_D. Such a comparison is shown as an insert in Fig. 9, based on a compilation of data from the literature [9–12, 16] originally prepared by Livingood and Gauntner [30]. The present results seem to agree well with the mean of the correlations proposed in [9–12, 16], where the term $Re_b^{0.7}$ occurs in most of them and thus represents the dominant independent variable.

EXPERIMENTAL RESULTS, SEMICYLINDRICAL SURFACE

In the present results, there appears a different mode of dependence on Z_n/D, that is now the distance between the plenum chamber and the axis of symmetry of the cylinder, for $2 \leq Z_n/D \leq 8$, and shows up in the form of a term $(Z_n/D)^{-0.22}$. It indicates effectively a diminution of the cooling effect with the distance from the impingement plate (similar to the results of [9]. for example), because of a different potential core length, and a lack of opportunity to entrain the air from the surroundings for cooling purposes. Potential core length was not measured here because of the experimental difficulties of working in a very restricted space, but Jachna's measurements [24] show for it a tendency to decrease in a hemispherical cavity. Interference effects from the neighboring jets show up in the form of the term $(C_n/D)^{-0.16}$.

The most significant effect of the severely constricted geometry of the space between the plenum chamber and the impinging plate with a curvature is perhaps the extension of the area where stagnation flow prevails (with $Re_D^{0.5}$ term still applicable) and the fact that, at least for small Z_n/D values, a true wall-jet flow cannot develop, because of the restricted free space available between the impinging surface and the exterior of the plenum chamber, which could show itself in a change of the overall power of Re_D in the expression for the average Nusselt number. The above restriction on the

available free flow space, plus the fact that the ends of the testing surface were blocked off for the flow of air, imply for low Z_n/D values a possibility of formation of a channel-like flow away from the stagnation line as is suggested in [13]. This assessment of the flow situation in the space between the impingement surface and the plenum chamber is also supported by the calculations carried out in [15].

In the large scale configuration, there appear four identifiable areas of interest: (1) the heat transfer at the stagnation point – an average of three calorimeters, each one exposed to the full effect of jet centered on the particular calorimeter; (2) heat transfer when some of the jets were not aligned with all the calorimeters due to the fact that C_n was variable, while calorimeters were fixed in their relative positions at 25.4 mm center-to-center; (3) the local heat-transfer distribution, and (4) the average heat transfer (Figs. 9–12).

Because all the calorimeters remained in a fixed position relative to each other (as shown in Fig. 6), in the central one fifth portion of the target plate, while the nozzles used were spaced two, four, and eight nozzle diameters center-to-center (forming an integral part of the plenum chambers), the results required a careful interpretation of some of the findings. The effects of inevitable lack of complete alignment between the calorimeters and the nozzles in some instances were reduced, in relation to the average heat transfer, by a large number of surface-to-target distances, a wide Reynolds number range considered, and the fact that three nozzle diameters, and as many nozzle-to-nozzle spacings were used. The advantages of this experimental arrangement were a nearly complete elimination of end effects (of both fluid flow distribution and heat transfer), and a substantial reduction of effects of local calorimetric measurement errors.

It was to be expected, however, that local effects caused by calorimeter-versus-nozzle misalignments would be picked up by calorimeters located in the areas of particular interest, like, for example, the ones placed along the stagnation line. The physical significance of such measurements will be discussed below.

At the stagnation point, it is convenient to introduce a new dimensionless parameter, known as the Froessling number $Fr = Nu/Re^{1/2}$. Thus, the present large-scale configuration results yield a Froessling number that can be written in the form

$$Fr = 1.6\, Pr^{0.39}\, (D_c/D)^{-0.42} \times (Z_n/D)^{-0.22} (C_n/D)^{-0.16} \quad (15)$$

which shows that Fr is a function of the Prandtl number, the jet geometry, and the effects related to turbulence, shown by the last three parameters in equation (15) (Fig. 10). The fact that heat transfer in a row of jets is adversely affected by the term expressing the effect of interference of the other jets, C_n/D, appears to be logical. The negative power of (Z_n/D) is traceable to the restricted geometry at the bottom of the plenum chamber in the present test setup and the virtual

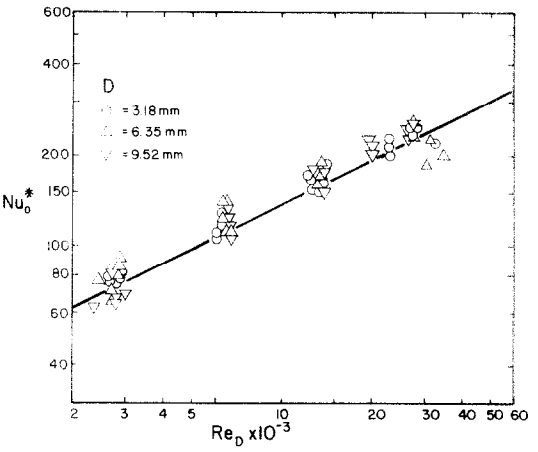

FIG. 10. Results at stagnation line according to equation (15): Nu_0^* vs. Re_D, semi-cylindrical plate results, $Nu_0^* = Nu_0\, Pr^{0.39}\, (D_c/D)^{0.42}\, (C_n/D)^{0.16}$.

inability to draw in additional air from the surroundings into a developing jet, between its emergence from the orifice and the point of impact, and before the wall jet has a chance to form. In all these aspects a single impinging jet is in a more favorable position, which shows up in the positive (Z_n/D) power (cf. equation (4) here). The dependence of Fr on $(D_c/D)^{-0.42}$ can be explained as a combined effect of turbulence intensity and of the turbulence scale normally associated with the size of the jet nozzle in the heat transfer from impinging jets for low Z_n/D-values. To isolate this effect, let's compare Fr from equation (15) with the corresponding experimental flat plate term, with (C_n/D) and (D_c/D) terms set equal to unity (cf. equation (5) and Fig. 7)

$$Fr = 1.42\, Pr^{0.39}\, (Z_n/D)^{0.16}. \quad (16)$$

It is seen from the direct comparison of these two equations that for $Z_n/D = 1.5$ (which, as mentioned above, is about the shortest distance at which jet flow at the orifice is not affected by the presence of the impingement plate), heat transfer at the stagnation point in the semicylindrical geometry is still virtually unaffected by the effects of curvature as expressed below by $Fr = 1.5\, Pr^{0.39}$ by both equations (15) and (16). A closer examination of the above experimental results shows existence of laminar-flow like heat transfer in its dependence on $Re_D^{0.5}$ (cf. equations (15) and (16), together with the expression for the boundary-layer thickness, equation (1)). The effects of turbulence outside of this 'viscous layer' make themselves felt, however, under the guise of a particular dependence on Z_n/D and D_c/D, and are affected substantially by the presence of curvature and the flow-constricting plenum chamber walls, in the case of a row of jets impinging on a semicylindrical plate [17, 22].

The stagnation line results for cases lacking align-

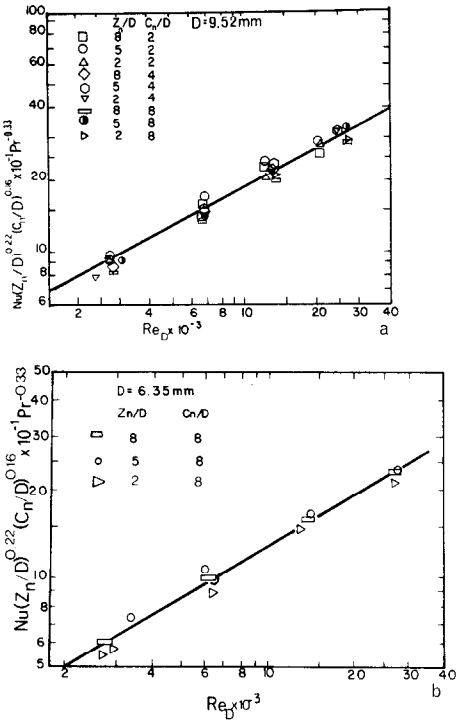

FIG. 11. Results at stagnation line, some calorimeter misalignment.

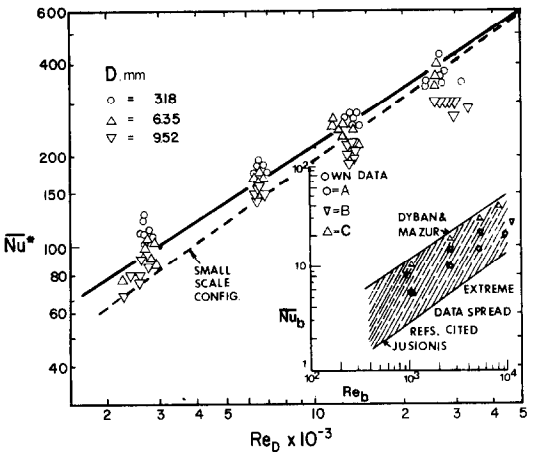

FIG. 12. $\overline{Nu}^*$ vs. Re_D, semi-cylindrical plate results, $\overline{Nu}^* = \overline{Nu}\, Pr^{0.33}\,(D_p/D)^{0.402}\,(C_n/D)^{0.16}$. Comparison with small scale configuration. Insert: comparison of semi-cylindrical plate results sith the references cited (not adjusted for effects of diameter). Diameter: A = 3.18 mm, B = 6.35 mm, C = 9.52 mm.

ment between the calorimeters and the jet nozzles are shown in Figs. 11(a) and 11(b). In Fig. 11a for D = 9.52 mm, the two outer calorimeters were spaced 6.35 mm from the nearest stagnation point, with the Nusselt number given by

$$Nu_o = 1.31\, Pr^{0.33}\, Re_D^{0.55} (Z_n/D)^{-0.22} (C_n/D)^{-0.16}. \quad (17)$$

Here, $Re_D^{0.55}$ appears to indicate a gradual deviation from the laminar stagnation point heat transfer. A calculation shows that Nu_o here is about 31% higher than that given by equation (15). In Fig. 11(b), the two outer calorimeters were at the midpoint between the two adjacent jets, and the correlating equation (for D = 6.35 mm, (C_n/D) = 8) is

$$Nu_o = 0.628\, Pr^{0.33}\, Re_D^{0.59} \times (Z_n/D)^{-0.22} (C_n/D)^{-0.16}. \quad (18)$$

Here, Nu_o is very nearly equal to the Nu_o resulting from equation (17), for $10^4 < Re_D < 3 \times 10^4$, and the effect of turbulence on heat transfer results in a substantial increase of the power of Re_D. The effect of stagnation line results on the average heat transfer should be negligible, however, because of a relatively small area involved in most cases. Still, because of only three calorimeters' taking care of a large number of nozzles, such misalignment can furnish new information for heat transfer at stagnation line like, e.g., the existence of a secondary absolute maximum away from stagnation point.

The local distribution of heat-transfer coefficient is shown in Fig. 9. It is seen that, at 45° angular distance from stagnation point, there occurs a kind of a secondary maximum of heat transfer that appears to be strongly dependent on the Reynolds number, and has been observed by other investigators (Schlünder *et al.* [4], Koopman and Sparrow [5], Gardon *et al.* [1, 3] and Dyban and Mazur [13]) in connection with impinging jets, for relatively short nozzle-to-plate distances (theoretically unexplained).

The average heat transfer for $2 \le Z_n/D \le 8$ is shown in Fig. 12. It follows the equation (with the $Pr^{0.33}$ term adapted from the Colburn analogy, equation (10)).

$$\overline{Nu} = 0.72\, Pr^{0.33}\, Re_D^{0.63} \times (C_n/D)^{-0.16} (D/D_p)^{0.402}. \quad (19)$$

Equation (19) shows a dependence of the average Nusselt number on a relatively low power n of Re_D, explainable by a larger extent of stagnation are a heat transfer with n = 0.5, due perhaps to the restricted air entrainment from the surroundings, and the possibility that instead of typical wall jet flow, discussed above, a hybrid form of flat plate-wall jet flow was actually forming, with the critical Reynolds number being a function of the distance. It is characteristic that small-scale configuration equation, with $Z_n/D \le 8$, could still clearly produce a $Re_D^{0.7}$ term as the form of functional dependence on the Reynolds number, similar to the calculated, and also experimentally verified power of Re_D correlation led to n = 0.7; when the effects of 'misalignments' had to be included they expressed themselves in such a distribution of the data points that led eventually to lowering of the power n. On the average, this would produce $n = 0.6^+$, as the average

data on $\overline{Nu}$ have, so far, substantiated as shown in equation (19). It appears, therefore, that for a fixed spacing of the calorimeters, and a variable spacing of the nozzle orifices, the resulting correlations would be expected to be responsive to all thus induced changes of the flow regime, which will manifest themselves in changes of the power of the applicable Reynolds number. Characteristic of the average data is the absence of Z_n/D terms for $2 \leq Z_n/D \leq 8$ which is, again, consistent with the flat plate data. It is believed that large number of data taken with 21 calorimeters should have produced representative overall average values (cf. [9–13, 16, 17 and 30]), useful both for research and development and design purposes.

A final cross-checking of the average heat-transfer data here may be made by a direct comparison of equations (14) and (19). Except for the Z_n/b term, equation (14) is already in the form suitable for such a comparison. An appropriate choice of Z_n/b is 16.9, corresponding to $Z_n/D = 2$, that takes us well into the range of validity of equation (19), and yields the expression shown in Fig. 12 and below

$$\overline{Nu}^*_{D,ssc} = \overline{Nu}_{D,ssc}\left[(C_n/D)^{0.16}\,(D/D_p)^{-0.402}\right] = 0.337\,Re_D^{0.7}\,Pr^{0.33} \qquad (20)$$

obtained with Z_n/b raised to -0.32 power that makes small-scale configuration results look essentially equivalent to semicylindrical plate data in the higher Reynolds number range of the values tested, but somewhat lower for the smaller Reynolds numbers listed in Fig. 12. Here, the agreement between the two sets of data is obtained through averaging of powers of Z_n/D occurring in equations (14), ($n = -0.42$, $Z_n/D > 8$), and (15), ($n = -0.22$, $2 < Z_n/D < 8$) applicable for semicylindrical plate. Interesting is the reason for the difference in the power of the Reynolds number occurring in equations (14) and (19), however, since equation (19) yields an expression, analogous to that given by equation (20)

$$Nu^*_D = 0.72\,Re_D^{0.63}\,Pr^{0.33}. \qquad (21)$$

Some of these reasons are doubtless the constricted flow inside a cavity formed between the target plate and the plenum chamber [17, 22] for small Z_n/D values and the resulting lack of space for wall jet development. Therefore, it is interesting to report that equation (21) is quite similar to one proposed by Smirnov *et al.* [31] for heat transfer due to jet flow into the dead end of a cylinder.

DISCUSSION OF RESULTS

While the average data for small scale configuration have been already discussed and shown to fall about into the middle of the range of results presented by several investigators, the stagnation point data have been compared with a calculated result based on the first principles, and found to be essentially in full agreement (for $Z_n/D = 1.5$). The data on average heat transfer, for large scale configuration, run relatively high, just below the results of Dyban and Mazur [13, 17] and slightly above those of Metzger *et al.* [9]. From [17] it appears (cf. Refs. 99, 119, 244 and 384) that the above results of Dyban and Mazur have been checked in several ways and should be considered as essentially substantiated. The Refs. 244 and 384 of [17] are the present [10 and 11], and Ref. 99 is equivalent to [13]. For a comparison with [9–13], cf. Fig. 12 insert adapted from [30].

The usefulness of equation (19) may be illustrated by the following example: for $D = 9.52$ mm, $D_p = 127$ mm, $C_n/D = 2$, and $\bar{t} = 75°C$, equation (19) yields $h_1 = 244$ (at $Re_D = 15\,000$), $h_2 = 378$ (at $Re_D = 30\,000$, and $h_3 = 2440$ (at $Re = 10^6$), all in W m^{-2} K^{-1}; the values for h_1 and h_2 compare favorably with the range of heat transfer coefficients shown in Fig. 9 here. On the other hand, Shvets and Dyban [17], p. 326 cite as typical for the geometry, equivalent to that covered by equation (19), $3000 < h_4 < 5000$, in W m^{-2} K^{-1}, for $5 \times 10^4 < Re_D < 10^6$. Thus, the present equation (17) appears to give quite moderate and reasonable values for the range of its experimental validity, $10^4 < Re_D < 30\,000$, as well as when directly extrapolated to $Re_D = 10^6$, since $h_3 < h_4$, at any rate.

Dyban and co-workers have used techniques stressing the fundamental fluid flow aspects of impinging jets, combined with direct heat-transfer measurements, roughly similar to the approach taken by the present author.

It has been emphasized throughout this paper that, at the stagnation point, there exists a basic similarity in fluid flow and heat-transfer characteristics between the flat and cylindrical target plates. Therefore, preliminary results obtained with a flat plate have been also discussed. The present results at the stagnation point are similar to those of Brdlik and Savin [32] and to those of Chia *et al.* [33] who like, for example, Koopman and Sparrow [5] used mass-transfer analogy. Average heat-transfer data in the impingement region have been obtained by Yokobori *et al.* [34], who used water as their fluid; they are somewhat lower than the present stagnation point results. The average flat plate results (Fig. 5) yield $240 < \bar{h} < 670$ W m^{-2} K^{-1} for $14\,000 < Re_D < 67\,000$, which is comparable to the average semicylindrical plate results (Fig. 12, equation (19)).

It is believed that the relatively high heat transfer rates, with respect to those in [9–12, 16], are to some extent due to a high level of turbulence caused by the metal sieves and glass wool inside of the plenum chambers used. The metal sieves and glass wool were originally installed in order to equalize flow among the individual nozzles, but their total contribution may have been not very different from that of the turbulizers described in [22], for example, resulting in somewhat higher average heat-transfer rates.

The magnitude of the local heat-transfer coefficients shown in Fig. 9 compares favorably with the values obtained, for example, by Bouchez and Goldstein [6].

An additional analysis of local heat-transfer coefficients may be found in [2], where comparison of the present data with heat transfer from jets impinging on hemispherical surfaces is also made. The present results show actually the need for some changes in the geometry, and for the use of turbulence promoters, to increase the intensity of heat transfer from air jets impinging into a cavity. This will require additional research on fluid flow in curved channels, and on further effects of jets impingement on various curved surfaces (cf. [8] and [17]). For high-temperature cooling applications, the effects of variable properties will have to be introduced [29] to make the final results more realistic. There exist basic similarities between the jets, impinging on flat and curved (concave and convex) surfaces. The unique geometry and crowding that prevails in typical applications of impinging jets towards cooling of turbine blades cannot be fully generalized, however, and will require some specialized testing in particular cases of interest for the best possible results. The effects of turbulence scale may show in the scaled-up versions of the typical applications. It appears that intensity of heat transfer from impinging jets may reach levels as high as 10 000 $W m^{-2} K^{-1}$ [17], that have been ordinarily associated with evaporative cooling. This fact makes future applications of impingement cooling particularly attractive, and is indicative of the immediate research needs in that area.

SUMMARY

Starting with the velocity profiles and the boundary layers at the stagnation point and in the wall-jet region, expressions for heat transfer have been derived from the Froessling's solution of the governing equations and from the Colburn analogy. These results were then compared with experimental findings. It has been shown that flat plate results, obtained with a single jet, can be, with certain modifications, applied also to a row of jets impinging on a semicylindrical surface.

Average Nusselt numbers, obtained with a set up scaled down ten times, were compared with the Nusselt numbers (average and local), resulting from measurements on a semicylindrical surface 254 mm long and of 127 mm dia., exposed to a row of jets. Comparisons with the results of a number of other investigators were also made, with generally satisfactory results. The heat-transfer intensities were high, but still well below the maximum values stated in the literature on impingement cooling of concave surfaces.

Acknowledgement—The author wishes to acknowledge the support of the M.E. Department Staff and help of Drs. R. Y. Chen and R. Nagarajan in collection and processing of data. Also, this work has been partially supported under contract NAS3-11175.

REFERENCES

1. R. Gardon and J. Cobonpue, Heat transfer between a flat plate and jets of air impinging on it, in *International Developments in Heat Transfer*, ASME, pp. 459–460 (1963).
2. P. Hrycak, Heat transfer from a row of jets impinging on concave semi-cylindrical surface, in *Proc. 6th International Heat Transfer Conference*, Vol. 2, pp. 67–72, EC-11, Toronto, Canada (1978).
3. R. Gardon and J. C. Akfirat, The role of turbulence in determining the heat transfer characteristics of impinging jets, *Int. J. Heat Mass Transfer* **8**, 1261–1272 (1965).
4. E. U. Schlünder, P. Krötzsch and W. Hennecke, Gesetzmässigkeiten der Wärme und Stoffübertragung bei der Prallströmung aus Rund und Schlitzdüsen, *Chem. Ing. Tech.* **42**, 333–338 (1970).
5. R. N. Koopman and E. M. Sparrow, Local and average transfer coefficients due to impinging jets, *Int. J. Heat Mass Transfer* **19**, 673–683 (1976).
6. J. P. Bouchez and R. J. Goldstein, Impingement cooling from a circular jet in cross-flow, *Int. J. Heat Mass Transfer* **13**, 719–730 (1975).
7. J. N. B. Livingood and P. Hrycak, Impingement heat transfer from turbulent air jets to flat plates. A literature survey, NASA TM X-2778 (1973).
8. H. Martin, Heat and mass transfer between impinging gas jets and solid surfaces in *Advances in Heat Transfer*, Academic Press, New York. Edited by J. P. Hartnett and T. F. Irvine Jr. Vol. 13, pp. 1–60 (1977).
9. D. E. Metzger, T. Yamashita and C. W. Jenkins, Impingement cooling of concave surfaces with lines of circular air jets, *J. Engng Pr* **91**, 149–158 (1969).
10. R. E. Chupp, H. E. Helms, P. W. McFadden and T. R. Brown, Evaluation of internal heat transfer coefficients for impingement-cooled turbine airfoils, *J. Aircraft* **6**, 203–208 (1969).
11. C. W. Jenkins and D. E. Metzger, Local heat transfer characteristics on concave cylindrical surfaces, Tech. Rept., ME-694, Arizona State Univ. (1969).
12. V. J. Jusionis, Heat transfer from impinging gas jets on an enclosed concave surface, *J. Aircraft* **7**, 87–88 (1970).
13. Ye. P. Dyban and A. I. Mazur, Heat transfer from a flat air jet flowing into a concave surface, *Heat Transfer – Soviet Res.* **2**, 15–20 (1970).
14. W. Tabakoff and W. Flevenger, Gas turbine blade heat transfer augmentation by impinging air jets having various configurations, *J. Engng Pr* **94**, 51–60 (1972).
15. L. L. Debruge and L. L. Han, Heat transfer in a channel with porous wall for turbine cooling application, *Journal Heat Transfer* **94**, 385–390 (1972).
16. F. Burggraf, Local heat transfer coefficient distribution with air impingement into a cavity, Paper 72-GT-59, ASME (1972).
17. I. T. Shvets and Ye. P. Dyban, *Air Cooling of Gas Turbine Elements* (in Russian), Naukova Dumka, Kiev.
18. M. Poreh, Y. G. Tsuei and J. E. Cermak, Investigation of a turbulent radial wall jet, *J. Appl. Mech.* **34**, 457–463 (1967).
19. D. T. Lee, Experimental investigation of submerged, incompressible turbulent, impinging jets, M. S. Thesis, N.C.E., Newark, NJ (1969).
20. P. Hrycak, D. T. Lee, J. W. Gauntner and J. N. B. Livingood, Experimental flow characteristics of a single turbulent jet impinging on a flat plate, NASA TN D-5690 (1970).
21. P. Hrycak, S. Jachna and D. T. Lee, A study of characteristics of developing incompressible, axisymmetric jets, *Lett. Heat Mass Transfer* **1**, 67–72 (1974).
22. Ye. P. Dyban and A. I. Mazur, Heat transfer near stagnation point in a turbulized impinging stream, *Thermal Physics and Heat Technology* (in Russian) **33**, 6–11 (1977).
23. P. Hrycak and S. Jachna, Environmental impact of submerged turbulent plumes, in *Proc. Inst. Environmental Sciences*, pp. 538–542 (1976).
24. S. Jachna, Axisymmetric air jet impinging on a hemispherical concave plate, Sc. D. Dissertation, N.J.I.T.,

Newark, NJ (1978).
25. D. Chan, Axisymmetric air jet impinging on a convex hemispherical plate, M.S. Thesis, N.J.I.T., Newark, NJ (1979).
26. H. Schlichting, *Boundary-Layer Theory*, 7th ed. McGraw-Hill, New York (1979).
27. E. R. G. Eckert and R. M. Drake, Jr., in *Heat and Mass Transfer*, p. 148. McGraw-Hill, New York (1959).
28. M. Sibulkin, Heat transfer near the forward stagnation point of a body of revolution, *Jl. Aeronaut. Sci.* **19**, 570–571 (1952).
29. J. Vilemas, B. Česna and V. Survila, *Heat Transfer in Gas-Cooled Annular Channels* (in Russian) Mokslas, Vilnius (1977).
30. J. N. B. Livingood and J. W. Gauntner, Average heat transfer characteristics of a row of circular air jets impinging on a concave surface, NASA TM X-2657 (1972).
31. V. A. Smirnov, G. E. Verevochkin and P. M. Brdlick, Heat transfer between a jet and a held plate normal to flow, *Int. J. Heat Mass Transfer* **2**, 1–7 (1961).
32. P. M. Brdlik and V. K. Savin, Heat transfer between an axisymmetric jet and a plate normal to the flow, *Inzh.-Fiz. Zh.* **8**, 146–155 (1965).
33. C. J. Chia, F. Giralt and O. Trass, Mass transfer in axisymmetric turbulent impinging jet, *I/EC Fundamentals* **16**, 28–35 (1977).
34. S. Yokobori, N. Kasagi, M. Hirata, M. Nakamaru and Y. Haramura, Characteristic behaviour of turbulence and transport phenomena at the stagnation region of an axisymmetrical, impinging jet, paper presented at the 2nd International Sumposium on Turbulent Shear Flows, London (1979).
35. W. Schach, Umlenkung eines kreisförmigen Flüssigkeitstrahles an einer ebenen Platte senkrecht zur Strömungsrichtung, *Ingr Archiv* **6**, 51–59 (1935).
36. T. Strand, On the theory of normal ground impingement of axi-symmetric jets in inviscid incompressible flow, AIAA Paper No. 64–424 (1964).
37. W. G. Brady and G. Ludwieg, Theoretical and experimental studies of impinging uniform jets, *J. Am. Helicopter Soc.*, **8**, No. 2, 1–13 (1963).
38. H. Rouse and A. -H. Abdul-Fetouh, Characteristics of irrotational flow through axially symmetric orifices, *J. Appl. Mech.* **17**, 421–426 (1950).
39. H. Ludwieg and W. Tillmann, Untersuchungen über die Wandschubspannung in turbulenten Reibungsschichten, *Ingr Archiv* **17**, 288–299 (1949).

APPENDIX I

Determination of a^* for small Z_n/D values

The term $a^* = \Delta(v/u_{oc})/\Delta(r/D)$ at $r = 0$ can be determined from the analytical solution of a related potential flow problem by Schach [35] as $a^* \doteq 1.3$ for $Z_n/D = 1.5$ (cf. Fig. 10 of [35]). Independently, one can deduce from the results quoted by Strand [36] $a^* = 1.2$, and from those by Grady and Ludwieg [37], $a^* = 1.14$, both for $1 < Z_n/D < 2$. An additional estimate of the magnitude and form of a^* for $Z_n/D \approx 1$ can be obtained as follows. The coefficient of contraction for the potential flow from a slit in an infinite plane has been determined as $C = 0.611$ [38]. Then, for a frictionless, incompressible fluid impinging normally from a nozzle of dia. D onto a plane Z_n distance away, one can assume that some contraction coefficient C_n applies to each linear dimension of the curved side of a cylinder πDZ_n through which the fluid is deflected; the nozzle exit forms the top of this imaginary cylinder. Then, from the continuity equation, there results

$$(\pi DC_1)(Z_nC_2)v = (\pi/4)D^2u_{oc} \qquad (1\text{-A})$$

while at $r = D/2$, for the radial flow outside of the boundary layer, $v/u_{oc} \doteq 1/2a^*$, which, substituted in equation (1-A), and letting $C_1 = C_2 \doteq 0.611$, yields

$$a^* \doteq (2C^2Z_n/D)^{-1} \doteq 1.33/(Z_n/D) \qquad (2\text{-A})$$

which is reasonably compatible with the theoretical and experimental results above [35–38] that apply to nozzles with a square velocity profile (cf. nozzle in Fig. 1). For other types of nozzles, with a non-uniform velocity distribution, a^* would be higher, which fact most likely could result in a higher local heat-transfer rate at $r = 0$.

APPENDIX II

An alternate calculation of wall jet heat transfer in axisymmetric jets

An alternate calculation of $\overline{Nu}$ that involves mainly the wall-jet region appears to be possible, again based on the Colburn analogy, but using a friction coefficient $C_f = 0.246\,(v_m\theta/\nu)^{-0.268}\ 10^{-0.678\delta^*/\theta}$, due to Ludwieg and Tillmann [39], and suitable to the calculations of two-dimensional turbulent boundary layers. Here δ^* is displacement thickness, and θ, momentum thickness, equal here to $\delta/15$ and $7\delta/120$, respectively, for $v/v_m = (z/\delta)^{1/14}$ according to equation (6), yields $C_f/2 = 0.0206\,(v_m\theta/\nu)^{-0.268}$. Further substitution of $v_m = 1.4\,(r/D)^{-1.12}u_{oc}$ (cf. equation (8)), and for $\delta = 0.0175D\,(r/D)^{0.95}$ (cf. equation (9)), generates $Nu = 0.168\,Re_D^{0.732}\,Pr^{0.33}\,(r/D)^{-1.07}$ which, integrated over the entire plate with a radius $D_p/2$, is

$$\overline{Nu} = 0.760\,Re_D^{0.732}\,Pr^{0.33}\,(D/D_p)^{1.07} \qquad (1\text{-A})$$

that for $14\,000 < Re_D < 67\,000$ may be also written in the form reasonably close to equation (12) above (except for the value of the numerical constant)

$$\overline{Nu} = 1.07\,Re_D^{0.7}\,Pr^{0.33}\,(D/D_p)^{1.07}. \qquad (2\text{-A})$$

Considering the limitations of the Colburn analogy (all parameters used resulted from fluid flow measurements carried out with cold air, the agreement between equations (2-A) and (12), obtained from direct heat-transfer measurements, is encouraging. Additional research is obviously still needed, to determine the form of the friction coefficients in wall jets deemed best suitable for heat-transfer calculations. It appears that neither C_f by Poreh *et al.* [18] is entirely vindicated by independent experiments with wall jets, nor is C_f by Ludwieg and Tillmann entirely satisfactory, having been obtained originally for different flow conditions [26].

TRANSFERT DE CHALEUR POUR UNE RANGEE DE JETS INCIDENTS SUR DES SURFACES CONCAVES CYLINDRIQUES

Résumé—En partant des principes de base et avec un paramètre obtenu expérimentalement, on obtient une expression du transfert thermique dans la région d'arrêt valable pour des jets circulaires incidents. Les résultats obtenus avec une rangée de jets d'air frappant une surface chauffée électriquement dans un montage qui simule à petite échelle une aube de turbine, sont compatibles avec le transfert moyen pour une surface chauffée à la vapeur, de géométrie semblable et à l'échelle dix, et ils sont comparables avec les résultats obtenus par d'autres auteurs. Ces observations sont attachées aux champs d'écoulement tels qu'ils existent dans les aubages de turbine à gaz, refroidis par une rangée de jets cylindriques ou un jet unique de largeur équivalente. La valeur du coefficient de transfert obtenue ici avec les jets incidents approche celle qui est normalement associée à la convection forcée de l'eau et du refroidissement par évaporation.

WÄRMEÜBERGANG EINER REIHE RUNDER STRAHLEN BEIM AUFTREFFEN AUF EINE KONKAVE ZYLINDRISCHE FLÄCHE

Zusammenfassung — Ausgehend von elementaren Ansätzen und unter Verwendung eines experimentell bestimmten Parameters wird eine Beziehung für den Wärmeübergang am Staupunkt runder, senkrecht auftreffender Strahlen abgeleitet. Versuchsergebnisse, die an einer elektrisch beheizten, von einer Luftstrahlenreihe angeblasenen Fläche (von der Größe einer typischen Gasturbinenschaufel) erhalten wurden, erwiesen sich als in Übereinstimmung mit dem mittleren Wärmeübergang an einer geometrisch ähnlichen, aber zehnmal größeren dampfbeheizten Fläche und als vergleichbar mit den Ergebnissen anderer Forscher. Diese Untersuchungen wurden in Anlehnung an Vorstellungen über die möglichen Strömungsverhältnisse im Inneren von Gasturbinenschaufeln durchgeführt, die innen von einer Reihe runder Strahlen oder einem einzelnen Strahl äquivalenten Durchmessers gekühlt werden. Die Größenordnung des Wärmeübergangskoeffizienten, der sich hierbei durch Anblasen mit Luftstrahlen ergibt, nähert sich derjenigen, die man normalerweise bei Wasserkühlung mit erzwungener Konvektion oder Verdampfungskühlung erhält.

ТЕПЛОПЕРЕНОС ОТ СИСТЕМЫ СТРУЙ, УДАРЯЮЩИХСЯ О ВОГНУТЫЕ ЦИЛИНДРИЧЕСКИЕ ПОВЕРХНОСТИ

Аннотация — На основании первого закона и с помощью одного экспериментально определяемого параметра выведено соотношение для величины критического теплового потока в системе круглых импактных струй. Найдено, что экспериментальные данные, полученные при исследовании системы воздушных струй, ударяющихся о нагреваемую электрическим током поверхность, на небольшой установке, моделирующей типичную турбинную лопатку, совпадают со средними значениями величины теплового потока на десятикратно увеличенной, но геометрически подобной, поверхности, нагреваемой паром, а также с результатами, представленными другими авторами. Затем производилась подгонка результатов к полям течения, имеющим место на лопатках газовой турбины, охлаждаемой изнутри системой круглых струй или единичной струей эквивалентной ширины. Значения коэффициентов теплопереноса, полученные в настоящей работе с использованием импактных струй, близки к значениям, рассчитываемым в том случае, когда учитываются вынужденная конвекция воды и испарительное охлаждение.